Diffuse-interface model for nanopatterning induced by self-sustained ion-etch masking

Sébastien Le Roy, Elin Sondergard, Ingar S. Nerbo, Morten Kildemo, Mathis
Plapp

HAL Id: hal-00499414
https://hal.science/hal-00499414

Submitted on 12 Jul 2010

Diffuse-interface model for nanopatterning induced by self-sustained ion etch masking

S. Le Roy and E. Søndergård

Surface du Verre et Interfaces, UMR 125 CNRS/Saint-Gobain, 93303 Aubervilliers, France

I. S. Nerbø and M. Kildemo

Physics Department, Norwegian University of

Science and Technology (NTNU), NO-7491 Norway

M. Plapp*

Physique de la Matière Condensée,

École Polytechnique, CNRS, 91128 Palaiseau, France

(Dated: March 12, 2010)

Abstract

We construct a simple phenomenological diffuse-interface model for composition-induced nano-patterning during ion sputtering of alloys. In simulations, this model reproduces without difficulties the high-aspect ratio structures and tilted pillars observed in experiments. We investigate the time evolution of the pillar height, both by simulations and by *in situ* ellipsometry. The analysis of the simulation results yields a good understanding of the transitions between different growth regimes and supports the role of segregation in the pattern-formation process.

1

The exposure of many metal and semiconductor surfaces to a homogeneous flux of sputtering ions leads to the spontaneous emergence of structures on the nanometer scale [1], which can profoundly modify the surface properties. While this phenomenon holds great promises for low-cost and large-area applications in optics and electronics, its specific use for the design of new materials and bottom-up manufacturing processes is at present hampered by our incomplete knowledge of the underlying mechanisms of self-organization. Especially, the dot or pillar features obtained on several III-V semiconductors [2, 3] or on some metals [4] are intriguing. These systems exhibit structures of unusually high aspect ratio as well as tilted pillars whose emergence cannot be explained by the classical Bradley-Harper (BH) theory [5] based on the curvature dependence of the sputtering yield. Instead, several authors have suggested that these patterns arise from shadowing effects induced by composition variations at the surface. Two distinct mechanisms have been proposed. In metals, the patterning was ascribed to external seeding by deposition of components from the surroundings of the sample [6]. More recently, the phase segregation of Ga during sputtering was pointed out as a potential source for a self-supplied etching shield in Ga-Sb [7], which can account for the pillar growth on GaSb as well as on other III-V semiconductors.

For a theoretical understanding of the composition-driven patterning mechanisms, extensions of the BH theory have been developed that take into account the influence of the surface composition on the evolution of the morphology [8, 9]. However, in these models the surface geometry is described in terms of a univalued height function $h(x, y, t)$. As a consequence, tilted pillars (and more generally any morphology exhibiting overhangs) cannot be modelled. Furthermore, the development of evolution equations for h generally relies on a small-slope approximation (for a review, see [10]), which makes their application to high-aspect ratio structures questionable. A diffuse-interface model is an elegant way to overcome both of these difficulties. In such models, surfaces are represented as smooth profiles of a scalar quantity (in our case, density) with a small but finite width W. This avoids the numerical difficulties arising from the tracking of an interface and has made such methods hugely popular in many different areas (for reviews, see [11, 12]). Here, we formulate a diffuse-interface model for pillar formation in Ga-Sb which contains only a small number of ingredients, namely (i) a difference in sputtering yield between the two species, (ii) phase segregation of Ga, consistent with the equilibrium phase diagram, and (iii) diffusion of matter in the amorphous layer created by the ion impact. Despite its simplicity, the model is
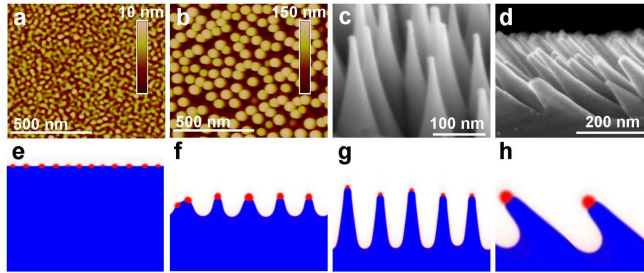
2

FIG. 1: (Color online) Evolution of the surface morphology during sputtering from experiments and simulations: (a) and (b) AFM images of the surface after 30 and 250 s, (c) cross section SEM image after 600 s, (d) cross section SEM image after 600 s of sputtering with 45° ion incidence, (e), (f), (g) simulation of the surface evolution for increasing sputtering times, Ga is represented in red and GaSb in blue, (h) simulation of the surface evolution with a 45° ion incidence.

capable of producing structures that bear a striking resemblance to those observed experimentally. Furthermore, the time evolution of the pillar height obtained from simulations reproduces well the experimentally observed three different growth regimes. The simulation results allow us to propose a refined physical interpretation of the pattern formation process.

In Figure 1a,b,c we show typical Atomic Force Microscopy (AFM) and Scanning Electron Microscopy (SEM) images of the surface morphology of GaSb after exposure to a 500 eV normal incidence Ar^+ ion beam. In the early stage of abrasion (30 s), the surface exhibits a pattern similar to those obtained during phase separation [13], see Fig. 1a. After 250 s, a dense pattern of pillars has formed, Fig. 1b. After 600 s, SEM images show high-aspect-ratio features with a spherical cap at the top. In Ref. [7], the cap was revealed to be a Ga-rich zone, and it was demonstrated that chemical variations precede the pattern formation. A simultaneous segregation and shielding mechanism was proposed based on these observations: the surface is enriched in Ga due to the difference in sputtering yield between Ga and Sb, and above a critical concentration, Ga segregates to form the Ga cap which acts as a sputtering shield. Since the difference in sputtering yield as well as the tendency for segregation are properties of the bulk material, the Ga-rich shield is resupplied during abrasion. This mechanism can explain why high aspect ratio structures readily form on GaSb, and also accounts for the tilted pillars reported for oblique ion incidence (see Fig. 1d and Refs. [7, 14]).

Our phenomenological model incorporates the salient features of the ion abrasion process,

without seeking a link to a microscopic description, which would be difficult to achieve in view of the complexity of the ion abrasion process. Note that our equations bear much similarity to mean-field kinetic equations for simple lattice-gas models that have been used previously to describe phase separation at surfaces [15]. The fundamental fields are the dimensionless number densities (that is, the number density times the atomic volume, assumed to be constant) $\rho_{\mathrm{Ga}}(\vec{x}, t)$ and $\rho_{\mathrm{Sb}}(\vec{x}, t)$. The dimensionless free energy of the system reads

$$F = \int \left[\frac{1}{2} W^2 (\nabla \rho_{\mathrm{Ga}})^2 + \frac{1}{2} W^2 (\nabla \rho_{\mathrm{Sb}})^2 + f_{\mathrm{tw}} \right] d\vec{x}, \tag{1}$$

with

$$
\begin{aligned}
f_{\mathrm{tw}} = \quad & \frac{1}{2} (\rho_{\mathrm{Ga}} + \rho_{\mathrm{Sb}})^2 (1 - \rho_{\mathrm{Ga}} - \rho_{\mathrm{Sb}})^2 + \frac{1}{2} (\rho_{\mathrm{Ga}} - \rho_{\mathrm{Sb}})^2 (1 - (\rho_{\mathrm{Ga}} - \rho_{\mathrm{Sb}}))^2 \\
& + 8 \rho_{\mathrm{Sb}}^2 (0.5 - \rho_{\mathrm{Sb}})^2 .
\end{aligned}
\tag{2}
$$

The potential f_{tw} has a triple-well shape, with the three minima corresponding to the three involved phases: $\rho_{\mathrm{Ga}} = \rho_{\mathrm{Sb}} = 0.5$ (GaSb), $\rho_{\mathrm{Ga}} = \rho_{\mathrm{Sb}} = 0$ (vacuum), and $\rho_{\mathrm{Ga}} = 1$, $\rho_{\mathrm{Sb}} = 0$ (pure Ga). The gradient terms induce smoothing of the surfaces over a characteristic thickness W. This functional generates three two-phase equilibria: between GaSb and vacuum, between pure Ga and vacuum, and between Ga and GaSb. Of course, this free energy is phenomenological and differs from the true thermodynamic free energy of the GaSb system. However, the only feature that is fundamentally necessary for our purpose is the room temperature coexistence of GaSb and Ga.

Next, we introduce sputtering and diffusion. Both processes are linked to the ion impact. Indeed, for the temperatures prevailing in our experiments (not too far above room temperature), bulk diffusion is virtually zero and even surface diffusion is slow, such that substantial mass transport occurs only due to energy transfer in the amorphous layer created by the ion impact, see figure 2a. To account for this fact, we introduce a dimensionless quantity $\xi(\vec{x}, t)$ which can be seen as the fraction of the initial energy still carried by the impacting ion at the position $\vec{x}$. It satisfies the equation

$$\xi(\vec{x}, t) = \max \left(0, 1 - \frac{1}{L} \int (\rho_{\mathrm{Ga}}(\vec{r}(s), t) + \rho_{\mathrm{Sb}}(\vec{r}(s), t)) \, ds \right), \tag{3}$$

where L is the penetration depth of the ions, and $\vec{r}(s)$ is the ion trajectory ending at $\vec{x}$. This creates an approximately linear decrease of ξ in the material, as represented in the sketch on figure 2a. This is a very crude approximation and differs from the usual Gaussian shape
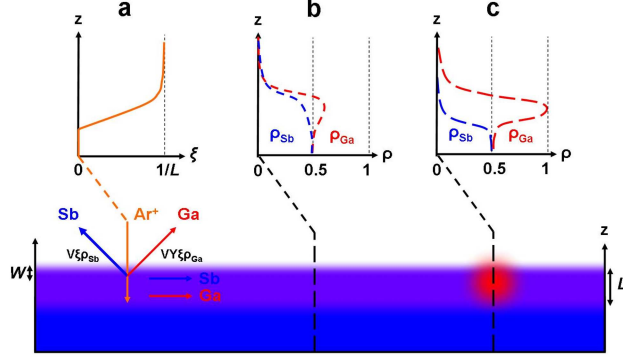
FIG. 2: (Color online) (a) Energy distribution ξ in the surface layer exposed to an ion beam, leading to the ejection of Ga and Sb and diffusion of atomic Sb and Ga. (b),(c) density profiles of a surface layer before and after segregation of a gallium droplet.

of the deposited energy used in the theory of Sigmund [16]. However, when the patterning process is composition-driven, the precise shape of the energy distribution is not important since the BH effect is not the principal driving phenomenon.

The evolution of the densities is then given by two equations accounting for diffusion and abrasion,

$$\frac{\partial \rho_i}{\partial t} = \vec{\nabla} \cdot \left[M_i(\xi, \rho_{\mathrm{Ga}}, \rho_{\mathrm{Sb}}) \vec{\nabla} \mu_i \right] - R Y_i \xi \rho_i \tag{4}$$

with $i = $ Ga or Sb,

$$\mu_i = \frac{\partial F}{\partial \rho_i} \tag{5}$$

the local chemical potential, R the sputtering rate of a flat Sb surface (proportional to the ion flux); $Y_{\mathrm{Sb}} = 1$ and $Y_{\mathrm{Ga}} = Y$ express the yield ratio between Ga and Sb. The mobilities are given by

$$M_i(\xi, \rho_{\mathrm{Ga}}, \rho_{\mathrm{Sb}}) = M_i^0 \xi \left(\rho_{\mathrm{Ga}} + \rho_{\mathrm{Sb}} \right)^2, \tag{6}$$

where M_i^0 are constants, the factor ξ accounts for the fact that diffusion is made possible by the ion impact, and the square of the total density suppresses spurious diffusion in the vacuum by evaporation-condensation, which is negligible under the conditions of our experiments. It is worth mentioning that, since we are using a dimensionless free energy functional, the constants M_i^0 have the dimensions of a diffusion coefficient.

The sputtering process is simulated by a simple finite-difference implementation of the above equations in a box with periodic boundary conditions on the lateral sides. The initial surface is defined as a pure GaSb phase ($\rho_{\mathrm{Ga}} = \rho_{\mathrm{Sb}} = 0.5$) in the lower part, and vacuum in

the top part ($\rho_{\text{Ga}} = \rho_{\text{Sb}} = 0$). A small random perturbation in both densities is added at the GaSb-vacuum interface, which generates small fluctuations of both surface height and surface concentration.

The parameter ranges for the quantities W, M_{Ga}^0, M_{Sb}^0, L, R, Y are selected as follows: W was set to the lattice constant of GaSb ≈ 0.6nm, a reasonable value for the unit cell; this parameter introduces a physical length scale in the system. The sputtering speed $RL/2$, calculated by the integration of the sputtering rate over the penetration depth, is used to introduce a time scale under the assumption of a certain flux (0.2 mA/cm^2) and yield (as estimated from the simulation of the sputtering process using the code TRIM [17]) which gives a sputtering speed of 0.46 nm/s. Y was taken between 0.4 and 0.5, which is small enough to obtain phase segregation. L ranges between 6 and 12 nm, a value close to the estimated penetration depth [17]. We took $M_{\text{Ga}}^0 = M_{\text{Sb}}^0 = M$ for simplicity, and chose 50 nm^{2}s^{-1} < M < 1000 nm^{2}s^{-1}.

Figure 1e,f,g show the time evolution of the surface morphology and the composition. The surface rapidly depletes in Sb due to the difference in sputtering yield between Ga and Sb, but remains almost flat. In this stage, the full diffuse-interface equations can be reduced to two coupled equations for the surface height and the surface composition which generalize those of Ref. [8]. The details of this procedure, as well as the linear stability analysis of the resulting equations, will be presented elsewhere. The most important findings are the following. For any yield ratio (including $Y = 1$) the BH instability occurs and leads to the slow exponential growth of structures with relatively large wavelengths. For sufficiently small yield ratio, the surface is enriched in Ga (Fig. 2b) until the interface concentration enters a concave region of the free energy landscape, and phase separation is triggered. The latter develops much faster than the BH instability, with a smaller characteristic wavelength, and leads to the formation of Ga-rich "droplets" (Fig. 2c) before the BH instability becomes visible.

Once Ga-rich droplets are formed, their coalescence is prevented by the increase of the surface relief, and well-defined structures are formed (Fig. 1e,f). The mobility is a decisive parameter at this stage, since it controls the size of and distance between the droplets. Upon further abrasion, high aspect ratio cones are formed, with a striking resemblance to observations by cross section SEM (Fig. 1c and g). This type of time evolution is obtained for a wide range of parameters. The mobility can vary over two orders of magnitude and
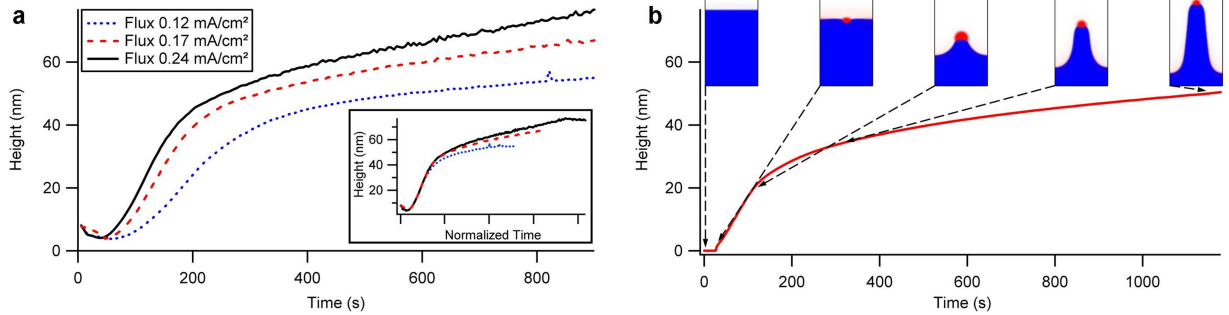
FIG. 3: (Color online) (a) Temporal evolution of the pillar height for various flux, obtained from experiments. The inset shows curves where the time was normalized to the length of the initial regime, i.e. the time to reach a height of 7 nm. (b) Simulated temporal evolution of the pillars and the corresponding morphologies, with $W = 0.6$ nm, $L = 6$ nm, $R = 0.15$ s^{-1}, $Y = 0.45$, and $M = 92$ nm^{2}s^{-1}.

the penetration depth from 6 nm to 12 nm with no change in the pattern stability. Finally, abrasion with a tilted ion incidence produces the same oblique structures as those observed in experiments (Figure 1d and h). Until now, models have failed in predicting such structures.

Real-time Spectroscopic Ellipsometry (SE) measurements were performed *in situ* during the sample abrasion in order to obtain the growth law of the features. The experiment and data interpretation are described in Ref. [14, 18]. The temporal evolution of the pillar height at 300 eV and various fluxes is shown in figure 3a. Three regimes are observed: First, a smoothing of the surface occurs. This corresponds to the abrasion of an oxide layer initially present on the surface. Next, a fast growth mode follows for around 1 minute before a slower growth mode establishes. No saturation of the slow growth has been observed even for samples sputtered 30 minutes [18].

Figure 3b shows the simulated height evolution together with typical surface morphologies. Since our model is phenomenological, we cannot expect quantitative agreement with the experiments. However, we do reproduce the three experimentally observed regimes, and the time and length scales have the correct order of magnitude. From the simulations, we can suggest the main mechanisms behind the three growth regimes. The first regime corresponds to the formation of a gallium-rich and unstable surface; the initial surface roughness is smoothed out. In the second regime, Ga segregation has occurred and the resulting droplets act as an etch mask. In this stage, the thickness of the Ga droplets is approximately equal

7

to the penetration depth. Therefore, the growth rate is directly given by the flux multiplied by the difference in sputtering yield between Ga and GaSb. This is supported by the fact that the second regime is best approximated by a linear law rather than an exponential expression, as previously suggested [18]. Both in the simulation and experiment, the slope indeed corresponds to the difference in yield between Ga and the GaSb substrate within the uncertainty on the physical parameters. This situation corresponds to the self-sustained etch masking mechanism proposed in [7] to explain the origin of the nanopatterns occurring on GaSb. The time scale of the first two regimes is directly proportional to the flux. This is evidenced from the experimental data by the existence of a master curve when the time is normalized by the duration of the first regime, see the inset of Fig. 3a.

The transition from the second to the third regime can be understood by analyzing the dynamic equilibrium between erosion and replenishing of the Ga droplets. The shielding Ga droplets are maintained by a supply of Ga from two sources. First, fresh Ga enters the droplet from the GaSb substrate directly underneath it. Second, the GaSb surface between the droplets continues to be enriched in Ga by the ongoing erosion, and excess Ga diffuses along the surface to join the droplets. However, the latter mechanism gets weaker as the amplitude of the structures increases, because the diffusion paths become longer. In the third regime, the diminishing Ga supply leads to thinner droplets, which means that the Ga cap does not completely shield against the sputtering ions. Therefore, the contrast in the sputtering yield between shielded and unshielded regions decreases, which leads to a slower growth of the pillars. This partial shielding regime can last for a long time, which explains why no saturation was found during the *in situ* height measurements. The normalized growth laws no longer fall on a master curve (Fig. 3a inset). It is difficult to obtain a general analytical expression for the growth rate in this regime, since it is determined by an interplay between etching and diffusion along a complex geometry, and thus depends on several parameters in a non-trivial way.

In conclusion, the above results show that a diffuse-interface model is a powerful method to investigate the effect of composition variation during ion sputtering. Our simple phenomenological model accounts for most of the specific features reported on GaSb, such as high aspect ratio structures and tilted pillars. The results of the simulations support the self-sustained shielding mechanism. They also bring new insights into the pillar formation process, and explain the overall shape of the observed growth laws. The simulations highlight

that the limiting factor in maintaining a self-sustained etch mask is the interplay between diffusion and a selective abrasion process. This controls the transition from complete to partial shielding.

Clearly, the simplicity of this method makes it a promising candidate to investigate new alleys for materials design by spontaneous pattern formation. In conjunction with more specific forms of the free energy as a function of composition, our approach can be used to investigate in a systematic way the interplay between the thermodynamic properties of materials and their pattern-forming ability.

---

* To whom correspondence should be addressed: `mathis.plapp@polytechnique.fr`

[1] W. L. Chan and E. Chason, J. of Appl. Phys. **101**, 121301 (2007).

[2] S. Facsko, T. Dekorsy, C. Koerdt, C. Trappe, H. Kurz, A. Vogt, and H. L. Hartnagel, Science **285**, 1551 (1999).

[3] Y. Yuba, S. Hazama, and K. Gamo, Nucl. Instrum. Methods Phys. Res., Sect. B **206**, 648 (2003).

[4] S. Rossnagel, R. Robinson, and H. Kaufman, Surf. Sci. **123**, 89 (1982).

[5] R. Bradley and J. Harper, J. Vac. Sci. Technol. A **6**, 2390 (1988).

[6] J. A. Sanchez-Garcia, L. Vazquez, R. Gago, A. Redondo-Cubero, J. M. Albella, and Z. Czigany, Nanotechnology **19**, 355306 (9pp) (2008).

[7] S. Le Roy, E. Barthel, N. Brun, A. Lelarge, and E. Søndergård, J. Appl. Phys. **106**, 094308 (2009).

[8] V. B. Shenoy, W. L. Chan, and E. Chason, Phys. Rev. Lett. **98**, 256101 (2007).

[9] R. Kree, T. Yasseri, and A.K. Hartmann, Nucl. Instr. and Meth. B **267**, 1403 (2009).

[10] M. Makeev, R. Cuerno, and A.-L. Barabási, Nucl. Instr. and Meth. in Phys. Res. B **197**, 185 (2002).

[11] L.-Q. Chen, Ann. Rev. Mater. Res. **32**, 113 (2002).

[12] I. Steinbach, Modell. Simul. Mat. Sci. Eng. **17**, 073001 (2009).

[13] C. D. Adams, M. Atzmon, Y.-T. Cheng, and D. J. Srolovitz, J. Mater. Res. **7**, 653 (1992).

[14] I. S. Nerbø, M. Kildemo, S. Le Roy, I. Simonsen, E. Søndergård, L. Holt, and J. C. Walmsley, Appl. Opt. **47**, 5130 (2008).

[15] M. Plapp and J.-F Gouyet, Phys. Rev. Lett. **78**, 4970 (1997), Eur. Phys. J. B **9**, 267 (1999).

[16] P. Sigmund, J. Mater. Sci. **8**, 1545 (1973).

[17] J. F. Ziegler, J. P. Biersack, and U. Littmark, *The Stopping and Range of Ions in Solids* (Pergamon Press, New York, 1985), new edition in 2009

[18] I. S. Nerbo, S. Le Roy, M. Kildemo, and E. Søndergård, Appl. Phys. Lett. **94**, 213105 (2009).